Electronic Supplementary Information

Enhanced rate and cyclability of porous $Na_3V_2(PO_4)_3$ cathode using dimethyl ether as electrolyte for application in sodium-ion batteries

Milan K. Sadan, Huihun Kim, Changhyeon Kim, Seung Hwan Cha, Kwon-Koo Cho, Ki-Won Kim, Jou-Hyeon Ahn*, Hyo-Jun Ahn*

Experimental

Materials and methods

Porous sodium vanadium phosphate (NVP) was synthesized by a sol–gel method; sodium hydroxide (NaOH, 98%, Alfa Aesar, Haverhill, Massachusetts, USA), ammonium vanadium oxide (NH_4VO_3, 99%, Alfa Aesar), ammonium dihydrogen phosphate ($NH_4H_2PO_4$, 99%, Acros Organics, Geel, Belgium), and citric acid ($C_6H_8O_7$, 98%, Sigma Aldrich, St. Louis, Missouri, United States) were dissolved in deionized water by magnetic stirring at 80 °C for 12 h. Then, the temperature of the obtained sol was increased to 120 °C until a gel was formed in the glass jar. The obtained gel was kept overnight in a vacuum oven at 80 °C. The as-obtained highly porous matrix was heated at 300 °C (ramp rate of 5 °C·min^{-1}) for 4 h for activation, followed by heating at 800 °C (ramp rate of 5 °C·min^{-1}) for 7 h in a tube furnace under a nitrogen atmosphere. The obtained powder was then washed several times with DI water and dried in an oven.

Material and electrochemical characterization

The crystallographic structures were analyzed using X-ray diffractometry (XRD; Bruker D8, Bruker Corporation, Billerica, Massachusetts, USA), and the morphology was observed using field-emission scanning electronic microscopy (FESEM, TESCAN (MIRA3 LM), Brno, Czechia) and transmission electron microscopy (TEM, JEOL 2010 FEG, JEOL Ltd., Tokyo, Japan). The porosity and surface area were measured using the Brunauer–Emmett–Teller (BET) method (Micrometrics Instrument Corporation (ASAP-2020M, Micrometrics), Norcross, Georgia, USA). The pore size was calculated by the Barret-Joyner-Halenda method (BJH). The carbon content was determined by elemental analysis (Flash 2000 CHNS/O analyzer, Thermo Fisher Scientific, Waltham, Massachusetts, USA). X-ray photoelectron spectroscopy (XPS; PHI 5000 VersaProbe, Ulvac-PHI, Inc., Kanagawa, Japan) was used to analyze the interface of the porous NVP electrode after the first cycle.
For electrochemical measurements, Swagelok-type cells were fabricated with Na metal as the counter electrode. Glass fiber separator (GF/D, Whatman™ PLC, Maidstone, UK) and Celgard 2400 were sandwiched as separators. Sodium hexafluorophosphate (1 M $NaPF_6$) in ethylene glycol dimethyl ether (DME), and 1 M sodium perchlorate ($NaClO_4$) in ethylene carbonate (EC)/propylene carbonate (PC) (1:1 V/V) and 5% fluoroethylene carbonate (FEC) were prepared in-house and used as electrolytes. For comparison, 1 M $NaPF_6$ in diethylene glycol dimethyl ether (DEGDME) and 1 M $NaPF_6$ in tetraethylene glycol dimethyl ether (TEGDME) were similarly prepared in-house. The cells were assembled in an argon-filled glove box and tested at room temperature. The electrode was prepared by mixing NVP, Ketjenblack, and polyvinylidene fluoride in an 8:1:1 ratio with *N*-methyl-2-pyrrolidone. The slurry was cast on carbon-coated aluminum foil with a loading of approximately 1 mg·cm^{-2}. All capacities were based on weight of NVP unless it was mentioned. The cycling of the cell was performed using a galvanostat (WBCS 3000L, WonA Tech Co. South Korea). Cyclic voltammetry and electrochemical impedance spectroscopy were performed using a VMP3 multi-channel potentiostat, (Biologic, Seyssinet-Pariset, France). The full cell was assembled with a Sn foil electrode with a mass ratio of 1:10, considering only the first voltage plateau of the Sn electrode. The energy density$_{cathode}$ of the full cell was calculated from the product of voltage and capacity$_{cathode}$ and energy density$_{total}$ was calculated based on the total weight of anode and cathode (real weight of anode= 5.0 mg and cathode =0.68 mg). Before assembling the full cell, the electrode was pre-cycled for two cycles to overcome the irreversible capacity. For ex situ XPS analysis, the cells were disassembled inside the glove box and washed with DME solution and dried under

vacuum. The sample was transferred to the chamber via a vacuum-filled chamber to prevent contamination with air.

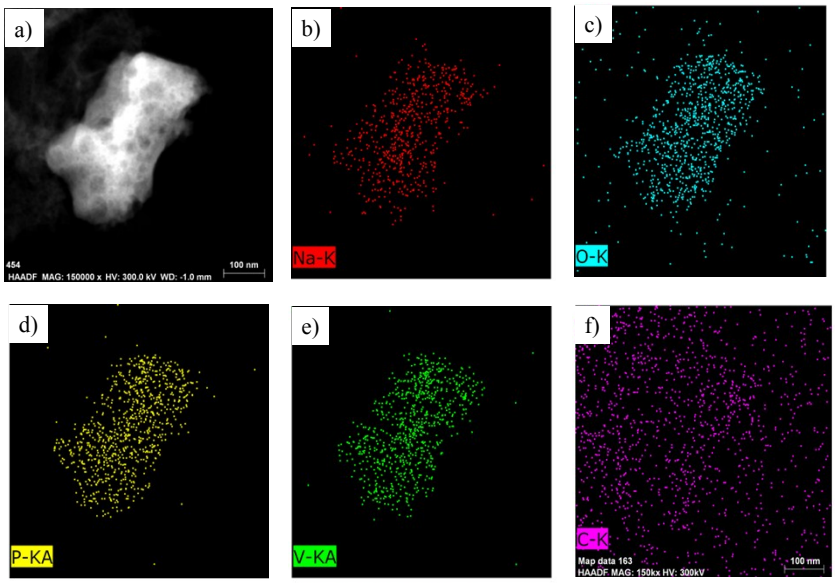

Figure S1. EDS Mapping of NVP, STEM mode.

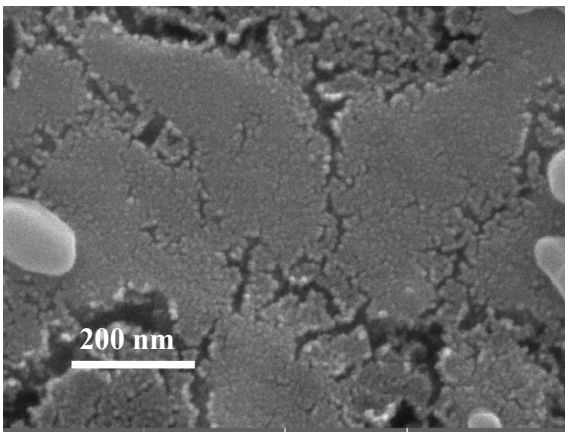

Figure S2. FESEM image of the NVP nanoparticles.

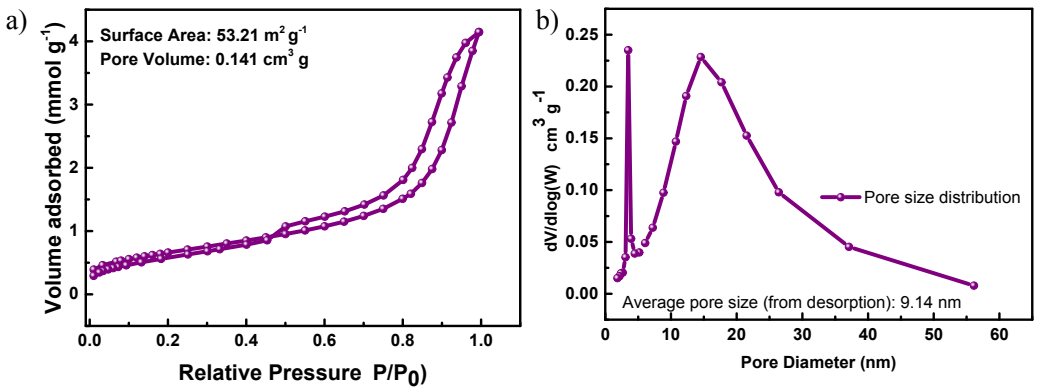

Figure S3. a) Nitrogen adsorption–desorption isotherm and b) pore size distribution of NVP nanoparticles.

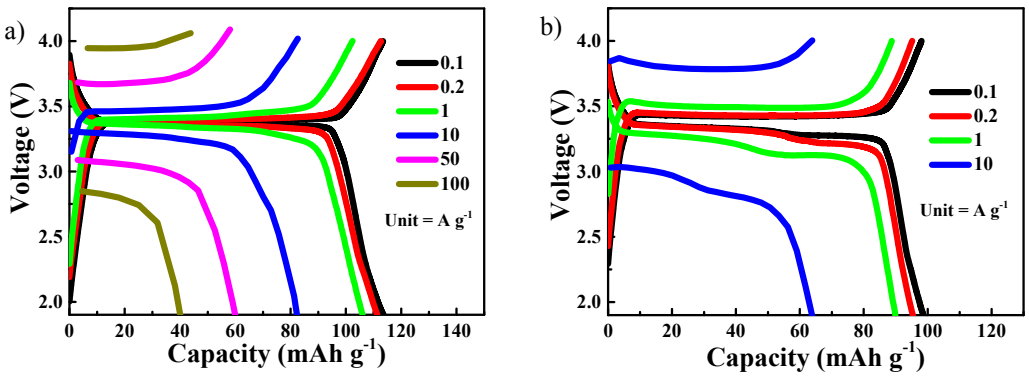

Figure S4. Voltage profile at different current densities with a) DME electrolyte and b) EC/PC electrolyte.

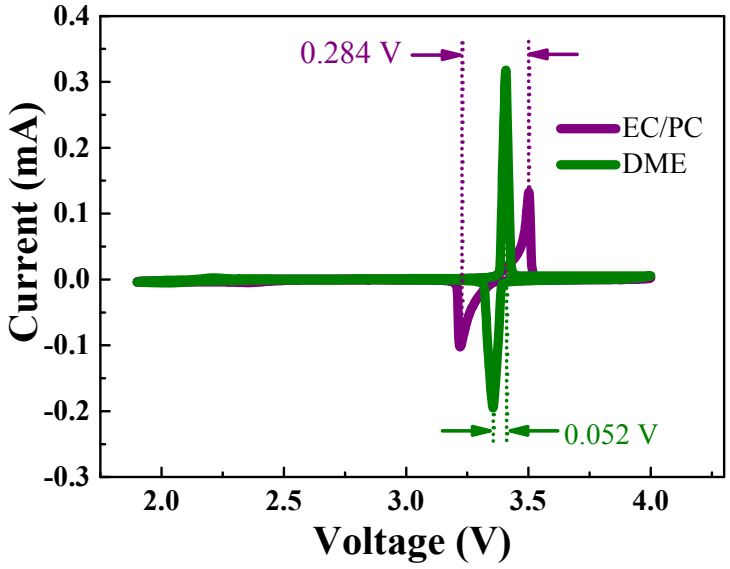

Figure S5. Cyclic voltammograms of the NVP electrodes with DME or EC/PC electrolytes at a scan rate of 0.05 $mV \cdot s^{-1}$.

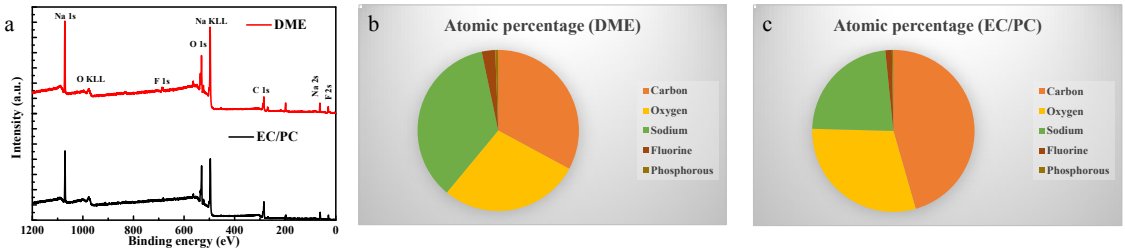

Figure S6. a) Ex-situ XPS survey spectra, b-c) atomic percentage of various elements in EC/PC and DME electrolyte respectively.

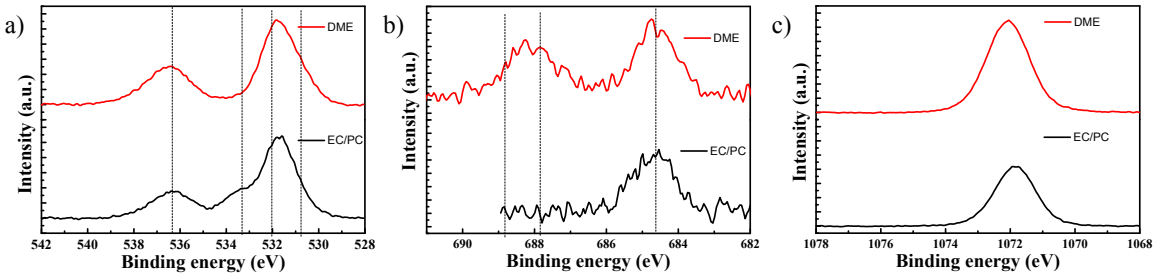

Figure S7. XPS of NVP electrode in carbonate: a) O 1s spectrum, b) F 1s spectrum, and c) Na 1s spectrum.

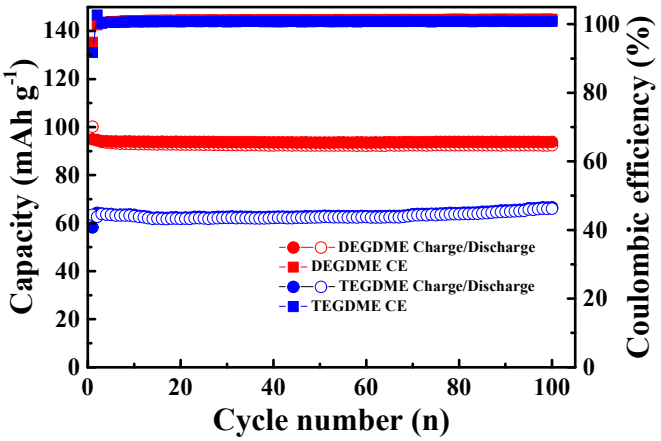

Figure S8. Solvent effects on cycling performance at a current density of 1170 mA·g^{-1} in DEGDME and TEGDME.

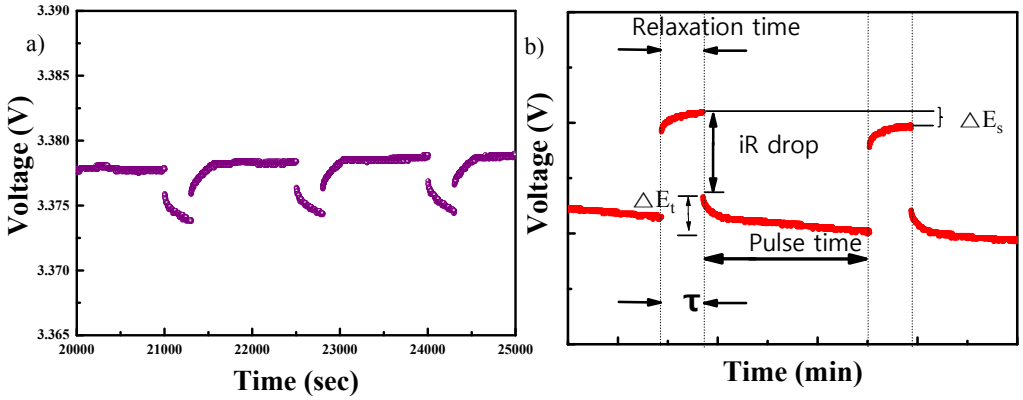

Figure S9. a) GITT profile of NVP in DME electrolyte during first cycle and b) typical GITT profile marked with the different parameters for calculation of diffusion coefficient.

Diffusion coefficient was calculated from Galvanostatic Intermittent Titration Technique (GITT) experiment by applying a constant current pulse with a relaxation time of 5 minutes. The diffusion coefficient is calculated by the following equation[35]:

$$D = \frac{4L^2}{\pi\tau}\left(\frac{\Delta Es}{\Delta Et}\right)^2$$

Where D is the diffusion coefficient (cm^2/s), τ is the relaxation time (s), ΔEs is the difference of the steady state voltage between two adjacent current pulse while relaxation time (V), ΔEt is the difference in potential change while pulse time discarding the iR drop (V). And L is the diffusion length (cm); for compact electrode, it's assumed to be the thickness of the electrode.

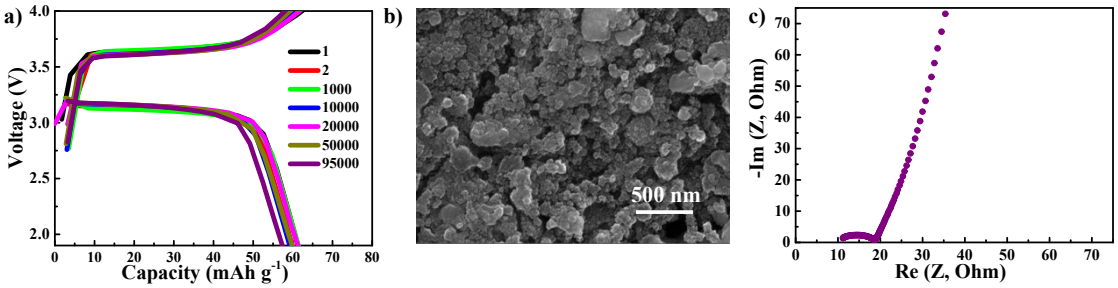

Figure S10. a) Selected voltage profile while cycling NVP electrode at 58.5 $A \cdot g^{-1}$ (500 C) in ether electrolyte, b) FESEM image of NVP electrode, and c) Nyquist plot after 95 000 cycles.

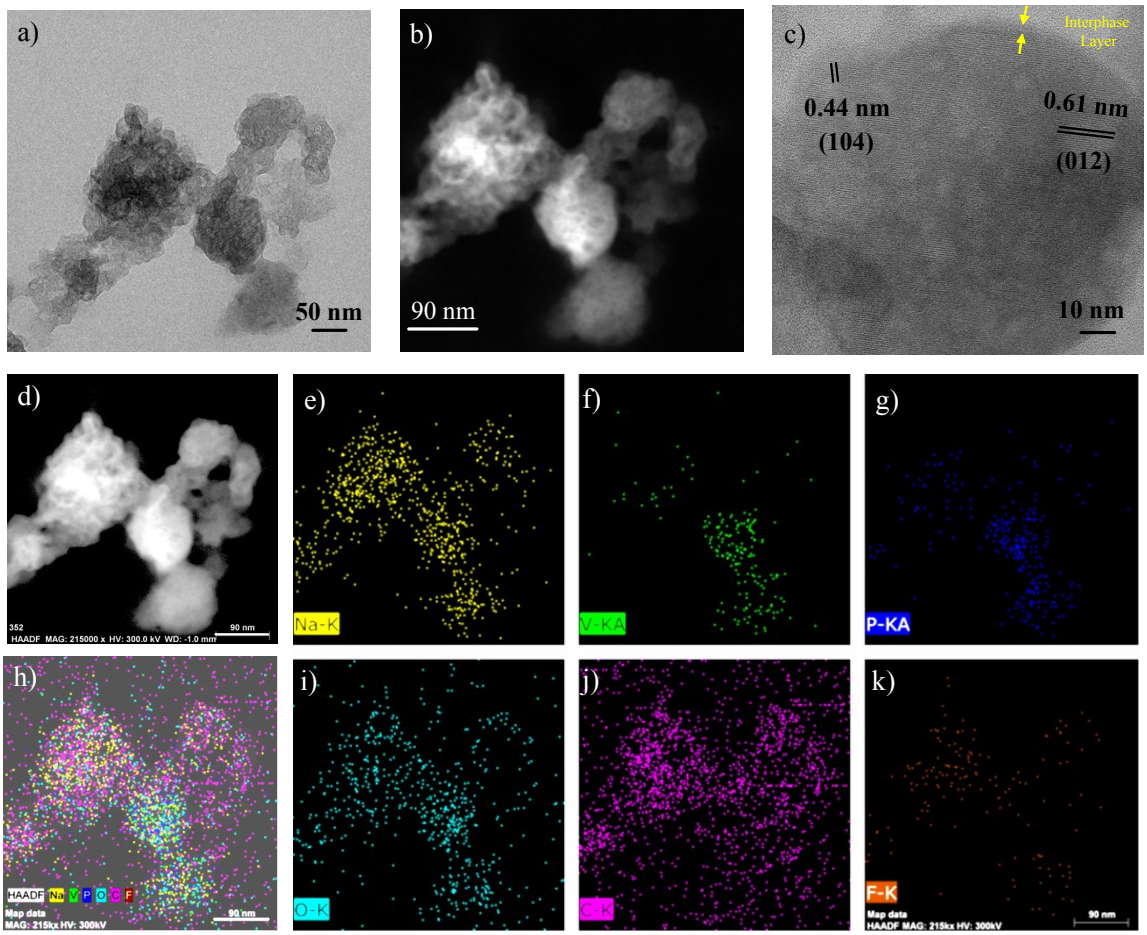

Figure S11. a) Ex-situ TEM image, b) STEM EDS, c) HRTEM image and d-k) EDS mapping of NVP after 95000 cycles

Figure S11a and b shows the TEM, and STEM images of the NVP after 95000 cycles. Even after 95000 cycles, NVP still have porous structure with similar size of the pristine NVP. Figure S11c shows the HRTEM image of NVP after 95000 cycles. The d spacing of 0.61 and 0.44 nm were observed which were corresponding to the (012) and (104) plane of NVP respectively. The crystal struture did not change by cycling. Additionally, a thin amorphous interphase layer was observed over the entire NVP particle which could be attributed to the electrode-electrolyte interphase. Figure S11 d-k shows the STEM mapping of the NVP after 95000 cycles. All the elements were uniformly distributed on the particle.

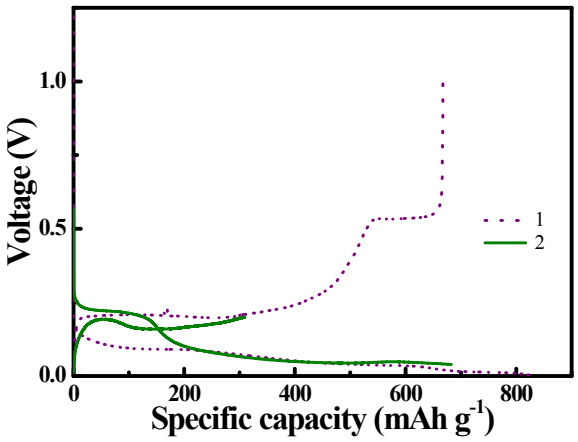

Figure S12. Voltage profile of the Sn electrode at a current rate of 84.7 mA·g^{-1} in the voltage scan range 0.001–1.0 V.

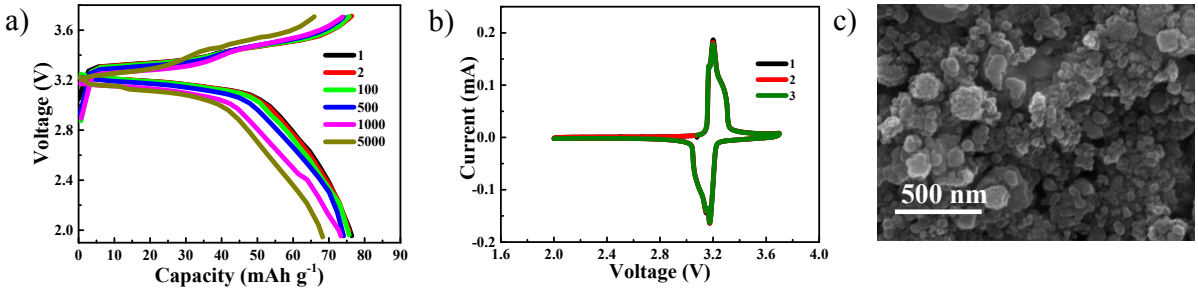

Figure S13. a) Voltage profile of full cell at a current density of 10 $A \cdot g^{-1}$ while cycling, b) cyclic voltammetry after 5000 cycles at a scan rate of 0.2 $mV \cdot s^{-1}$, and c) FESEM image of the NVP electrode in the full cell with a Sn electrode after 5000 cycles.

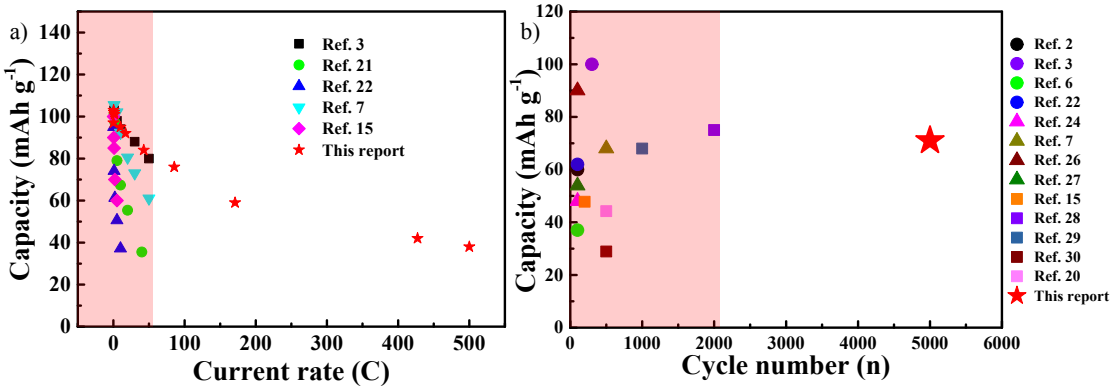

Figure S14. Comparison of a) rate performance and b) cycling performance of previous cathode limited full cell reports with our report.

Table S1. Comparison of previous NVP reports with high rate performance and/or long-term cycling performance.

Electrode	Electrolyte	Carbon content (%)	Voltage window (V)	Reversible capacity	Initial coulombic efficiency (%)	Cycling (rate, cycles)	Rate performance	Loading (mg/cm^2)	Ref.
Nano NVP/C	1 M $NaClO_4$ in PC	17	2.3–3.9	_	_	83 (10 C, 1000); 73 (50 C, 1000); 51 (100 C, 1000)	44 (22 A g^{-1})	1	1
3D interconnected NVP	1 M $NaClO_4$ in EC/DEC	7.93	2.5–4.0	~90 (15 C)	_	87 (15 C, 4000)	77 (150 C)		2
3D NVP nanofiber network	1 M $NaClO_4$ in EC/DMC + 5% FEC	6.7	2.3–3.9	100 (10 C)	90.9	95.9 (10 C, 1000)	94 (100 C)	1.5–2	3
NVP/C	1 M $NaClO_4$ in PC/FEC (95:5 v/v)	2.74	2.4–4.0	108 (0.2 C)	_	_	70 (100 C)	1	4
3D hierarchically porous NVP	1 M NaClO4 in EC/PC + 5% FEC	3.6	2.3–3.9	105 (0.1 C)	94	~90 (50 C, 30 000)	84 (400 C)	1.5–2	5
N, B codoped carbon coated 3D flower	1 M $NaClO_4$ in PC + 5% FEC	_	2.3–3.9	114 (1 C)	_	79 (100 C, 2000)	74 (100 C)	1–1.2	6
NVP@C anchored on carbon cloth	1 M $NaClO_4$ in EC/DMC + 5% FEC	8	2.0–3.9	116.6 (1 C)	90.8	95 (50 C, 2000)	69.9 (200 C)	5.38	7
NVP 3D foams	1 M $NaClO_4$ in PC + 5% FEC	22	2.5–3.8	112 (1 C)	97	70 (100 C, 1000)	51 (200 C)	_	8
NVP/C	1 M $NaClO_4$ in PC + 5% FEC	7.6	2.0–3.9	100.9 (1 C)	_	40 (200 C, 12 000)	55 (200 C)	_	9
NVP/C	2.1 M NaFSI/DME-BTFE (1:3)	10	2.7–3.7	~90 (12 mA g^{-1})	_	66.4 (2400 mA g^{-1}, 40 000)	~90 (1200 mA g^{-1})	1.5	10
3D porous NVP	1 M $NaClO_4$ in PC + 5% FEC	10.1	2.5–3.8	116 (0.5 C)	_	55 (100 C, 10 000)	86 (100 C)	0.8-1	11
NVP nanofibers	1 M $NaClO_4$ in PC/FEC (95:5 v/v)	6.95	2.6–3.8	_	_	~90 (20 C, 10 000)	76 (40 C)		12
NVP/C	1 M $NaClO_4$ in EC/DEC	6.41	2.8–3.8	115 (0.2 C)	_	~60 (30 C, 20 000)	38 (500 C)	1	13
NVP:rGO-CNT	1 M $NaClO_4$ in PC + 5% FEC	21%	2.3–3.9	~108 (100 C)	_	107 (10 C, 2000)	82 (100 C)	0.5–1	14
NaVP@rGO	1 M $NaClO_4$ in EC/DEC	3.28	2.3–3.9	112 (0.5 C)	_	~60 (30 C, 10 000)	79.2 (100 C)	1.5	15
NVP/C	1 M $NaClO_4$ in EC/PC	6	2.3–3.9	116 (0.1 C)	_	30 (40 C, 30 000)	61 (40 C)	3	16
NVP@rGO	1 M $NaClO_4$ in EC/DMC + 5% FEC	3	2.5–4.0	115 (0.5 C)	_	63 (50 C, 15 000)	41 (200 C)	1.5–2.0	17
NVP/C	1 M $NaClO_4$ in EC/DEC	7.25	2.0–4.0	117 (0.1 C)	_	55 (20 C, 10 000)	78 (20 C)	2	18
NVP/C	0.9 M $NaClO_4$ in TEP	_	2.3–4.0	_	_	72 (10 C, 10 000)	73 (30 C)	1.12	19
NVP microspheres	1 M $NaClO_4$ in PC + 5% FEC	9.72	2.5–4.0	117 (1 C)	98.8	86.6 (20 C, 10 000)	99.3 (100 C)	1.3	20
NVP/C	1 M $NaPF_6$ in DME	8	1.9–4.0	110	99	58.7	44	1 mg	Our

	(10 C)	(50 A g^{-1}, 95 000)	(854 C)	Report

Table S2. Fitting results of ex situ high-resolution XPS.

	Carbonate	Ether
C1s	290.15 eV (Na_2CO_3)	293.5 eV ($–CF_3$)
	288.95 eV (R-OCO_2Na)	289.3 eV ($–CF_2–$)
	286.85 eV (C–O)	286.85 eV (C–O)
	285.25 eV (C–C)	285.25 eV (C–C)
	284.2 eV (KB	284.2 eV (KB
O1s	531.11 eV (RCH_2ONa)	531.11 eV (RCH_2ONa)
	531.89 eV (Polyester)	531.89 eV (Polyether)
	533.41 eV (Na_2CO_3)	536.41 eV (Na KLL)
	536.41 eV (Na KLL)	
F1s	684.5 eV (NaF)	684.5 eV (NaF)
		687.8 eV (Na_xPF_y /$Na_xPO_yF_z$)
		688.85 eV (C–F)
Na 1s	1072.1 eV (Na–F/Na–O)	1072.1 eV (Na–F/Na–O)

Table S3. General properties of ether solvents.

	Chemical formula	Molar mass ($g \cdot mol^{-1}$)	Boiling point (°C)	Viscosity (cP)	Ionic conductivity ($\mu s\ cm^{-1}$) [34]	Dielectric constant
Ethylene glycol dimethyl ether (DME) 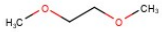	$C_4H_{10}O_2$	90.122	85	0.46	12890	7.18
Diethylene glycol dimethyl ether (DEGDME) 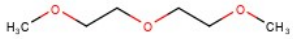	$C_6H_{14}O_3$	134.175	162	1.06	7320	7.4
Tetraethylene glycol dimethyl ether (TEGDME) 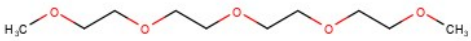	$C_{10}H_{22}O_5$	222.281	275	3.39	2580	7.53

Table S4. Comparison of the previous NVP full cell cathode limited reports.

Sl. No.	Electrode	Electrolyte	Anode	Cycling (cycles)	Rate performance	Ref.
1	3D interconnected NVP	1 M $NaClO_4$ in EC/DEC	HC	0.5 C, 60 mAh g^{-1} (100)	_	2
2	3D NVP nanofiber network	1 M $NaClO_4$ in EC/DMC + 5% FEC	NTP	5 C, ~100 mAh g^{-1} (300)	80 mAh g^{-1} @ 50 C	3
3	NVP/C	1 M $NaPF_6$ in EC/DEC + 5% FEC	NTFP/C	_	35.5 mAh g^{-1} @ 40 C	21
4	N, B co-doped carbon coated 3D flower	1 M $NaClO_4$ in PC + 5% FEC	NVP	1.1 A g^{-1}, 37 mAh g^{-1} (100)	45 mAh g^{-1} @ 40 C	6
5	$Na_2LiV_2(PO_4)_3$/C	1 M $NaClO_4$ in EC/DEC	HC	1 C, 62.19 mAh g^{-1} (100)	37.2 mAh g^{-1} @1.2 A g^{-1}	22
6	NVP	polymer electrolyte	SnS_2	1 C, 117 mAh g^{-1} (35)	_	23
7	NVP@C composite	1 M $NaClO_4$ in PC + 2% FEC	HC	1 C, 48 mAh g^{-1} (100)	_	24
8	NVP@C anchored on carbon cloth	1 M $NaClO_4$ in EC/DMC + 5% FEC	NTP	5 C, 68 mAh g^{-1} (500)	61 mAh g^{-1} @ 50 C	7
9	NVP/CNF	1 M $NaClO_4$ in PC + 2% FEC	NTP	20 mA g^{-1}, 50 mAh g^{-1} (16)	_	25
10	NVP/C	1 M $NaClO_4$ in PC	NVP	0.1 A g^{-1}, 90 mAh g^{-1} (100)	_	26
11	NVP:rGO-CNT	1 M $NaClO_4$ in PC + 5% FEC	NVP	1.1 A g^{-1}, 53.9 mAh g^{-1} (100)	_	27
12	NVP@rGO	1 M $NaClO_4$ in EC/DEC	HC	0.5 C, 59 mAh g^{-1} (50)	60 mAh g^{-1} @ 5 C	11
13	NVP@C core–shell	1 M $NaClO_4$ in PC	NVP	2 C, 73.6 mAh g^{-1} (50)	_	14
14	NVP@C@rGO	1 M $NaClO_4$ in PC + 5% FEC	NVP	3 C, 47.8 mAh g^{-1} (200)	38 mAh g^{-1} @ 10 C	15
15	$Na_3V_{2-x}Ca_x(PO_4)_3$@C	1 M $NaClO_4$ in EC/DMC + 5% FEC	NVP	10 C, 75 mAh g^{-1} (2000)	102 mAh g^{-1} @ 50 C	28
16	NVP@sulfur-doped carbon	1 M $NaClO_4$ in EC/DMC	NVP	5 C, 68 mAh g^{-1} (1000)	62 mAh g^{-1} @ 10 C	29
17	3D interconnected porous NVP	1 M $NaClO_4$ in PC + 5% FEC	NVP	5 C, 28.9 mAh g^{-1} (500)	47.7 mAh g^{-1} @ 5 C	30
18	NVP/C	0.9 M $NaClO_4$ in TEP	NVP	118 mA g^{-1}, 44.2 mAh g^{-1} (500)	35.1 mAh g^{-1} @ 1.88 A g^{-1}	20
19	NVP-CNT	1 M $NaPF_6$ in DEGDME	Bi	1000 mA g^{-1}, *76.7 mAh g^{-1} (400)	*85.15 mAh g^{-1} @ 4 A g^{-1}	31
20	NVP commercial	1 M $NaPF_6$ in DME	Bi@C	1000 mA g^{-1}, *60.5 mAh g^{-1} (500)	*32.6 mAh g^{-1} @ 10 A g^{-1}	32
21	NVP-CNT	1 M $NaPF_6$ in DEGDME	Sn	400 mA g^{-1}, *85.7 mAh g^{-1} (180)	*86.4 mAh g^{-1} @ 3.6 A g^{-1}	33
22	NVP/C	1 M $NaPF_6$ in DME	Sn foil	10 A g^{-1}, 71 mAh g^{-1} (5000)	38 mAh g^{-1} @ 58.5 A g^{-1}	Our Report

* Calculated value based on cathode mass

References

1 C. Zhu, K. Song, P. A. van Aken, J. Maier and Y. Yu, *Nano Lett.*, 2014, **14**, 2175.
2 W. Ren, X. Yao, C. Niu, Z. Zheng, K. Zhao, Q. An, Q. Wei, M. Yan, L. Zhang and L. Mai, *Nano Energy*, 2016, **28**, 216.
3 W. Ren, Z. Zheng, C. Xu, C. Niu, Q. Wei, Q. An, K. Zhao, M. Yan, M. Qin and L. Mai, *Nano Energy*, 2016, **25**, 145.

4 X. Jiang, T. Zhang and J. Y. Lee, *J. Power Sources*, 2017, **372**, 91.
5 T. Wei, G. Yang and C. Wang, *Nano Energy*, 2017, **39**, 363.
6 Y. Jiang, X. Zhou, D. Li, X. Cheng, F. Liu and Y. Yu, *Adv. Energy Mater.*, 2018, **8**, 1800068.
7 D. Guo, J. Qin, Z. Yin, J. Bai, Y.-K. Sun and M. Cao, *Nano Energy*, 2018, **45**, 136.
8 Y. Zhou, X. Rui, W. Sun, Z. Xu, Y. Zhou, W. J. Ng, Q. Yan and E. Fong, *ACS Nano*, 2015, **9**, 4628.
9 S. Li, P. Ge, C. Zhang, W. Sun, H. Hou and X. Ji, *J. Power Sources*, 2017, **366**, 249.
10 J. Zheng, S. Chen, W. Zhao, J. Song, M. H. Engelhard and J.-G. Zhang, *ACS Energy Lett.*, 2018, **3**, 315.
11 X. Rui, W. Sun, C. Wu, Y. Yu and Q. Yan, *Adv. Mater.*, 2015, **27**, 6670.
12 X. Jiang, L. Yang, B. Ding, B. Qu, G. Ji and J. Y. Lee*, J. Mater. Chem. A*, 2016, **4**, 14669.
13 Y. Fang, L. Xiao, X. Ai, Y. Cao and H. Yang, *Adv. Mater.*, 2015, **27**, 5895.
14 C. Zhu, P. Kopold, P. A. van Aken, J. Maier and Y. Yu, *Adv. Mater.*, 2016, **28**, 2409.
15 F. Li, Y.-E. Zhu, J. Sheng, L. Yang, Y. Zhang and Z. Zhou, *J. Mater. Chem. A*, 2017, **5**, 25276.
16 K. Saravanan, C. W. Mason, A. Rudola, K. H. Wong and P. Balaya, *Adv. Energy Mater.*, 2013, **3**, 444.
17 Y. Xu, Q. Wei, C. Xu, Q. Li, Q. An, P. Zhang, J. Sheng, L. Zhou and L. Mai, *Adv. Energy Mater.*, 2016, **6**, 1600389.

18 Q. Zhu, X. Chang, N. Sun, H. Liu, R. Chen, F. Wu and B. Xu, *J. Mater. Chem. A*, 2017, **5**, 9982.
19 X. Liu, X. Jiang, F. Zhong, X. Feng, W. Chen, X. Ai, H. Yang and Y. Cao, *ACS Appl. Mater. Interfaces*, 2019, **11**, 27833.
20 X. Cao, A. Pan, B. Yin, G. Fang, Y. Wang, X. Kong, T. Zhu, J. Zhou, G. Cao and S. Liang, *Nano Energy*, 2019, **60**, 312.
21 R. Klee, M. J. Aragón, R. Alcántara, J. L. Tirado and P. Lavela, *Eur. J. Inorg. Chem.*, 2016, **2016**, 3212.
22 M. Li, Z. Zuo, J. Deng, Q. Yao, Z. Wang, H. Zhou, W.-B. Luo, H.-K. Liu and S.-X. Dou, *J. Mater. Chem. A*, 2018, **6**, 9962.
23 J. Zheng, Y. Zhao, X. Feng, W. Chen and Y. Zhao, *J. Mater. Chem. A*, 2018, **6**, 6559.
24 X. Liu, E. Wang, G. Feng, Z. Wu, W. Xiang, X. Guo, J. Li, B. Zhong and Z. Zheng, *Electrochim. Acta*, 2018, **286**, 231.
25 Q. Ni, Y. Bai, Y. Li, L. Ling, L. Li, G. Chen, Z. Wang, H. Ren, F. Wu and C. Wu, *Small*, 2018, **14**, 1702864.
26 T.-F. Hung, W.-J. Cheng, W.-S. Chang, C.-C. Yang, C.-C. Shen and Y. -L. Kuo, *Chem. Eur. J.*, 2016, **22**, 10620.
27 P. Feng, W. Wang, K. Wang, S. Cheng and K. Jiang, *J. Mater. Chem. A*, 2017, **5**, 10261.
28 L. Zhao, H. Zhao, Z. Du, J. Wang, X. Long, Z. Li and K. Świerczek, *J. Mater. Chem. A*, 2019, **7**, 9807.
29 W. Li, Z. Yao, Y. Zhong, C. Zhou, X. Wang, X. Xia, D. Xie, J. Wu, C. Gu and J. Tu, *J. Mater. Chem. A*, 2019, **7**, 10231.
30 P. N. Didwal, R. Verma, C.-W. Min and C.-J. Park, *J. Power Sources*, 2019, **413**, 1.
31 C. Wang, L. Wang, F. Li, F. Cheng and J. Chen, *Adv. Mater.*, 2017, **29**, 1702212.
32 P. Xiong, P. Bai, A. Li, B. Li, M. Cheng, Y. Chen, S. Huang, Q. Jiang, X.-H. Bu and Y. Xu, *Adv. Mater.*, 2019, **31**, 1904771.
33 M. Song, C. Wang, D. Du, F. Li and J. Chen, *Sci. China Chem.*, 2019, **62**, 616.
34 M. Zhou, H. Tao, K. Wang, S. Cheng and K. Jiang, *J. Mater. Chem. A*, 2018, **6**, 24425.
35 G. Fang, Z. Wu, J. Zhou, C. Zhu, X. Cao, T. Lin, Y. Chen, C. Wang, A. Pan and S. Liang, *Adv. Energy Mater.*, 2018, **8,** 1703155.